APPLIED SCIENCES AND ENGINEERING

Concurrent stiffening and softening in hydrogels under dehydration

Shuai Xu[1]†, Zidi Zhou[1]†, Zishun Liu[1]*, Pradeep Sharma[2]

Hydrogels are an extraordinary soft matter system that serve as a laboratory for a rich plethora of multiphysical phenomena and find applications that range from biocompatible sensors to soft robots. Here, we report a peculiar experimental observation suggesting concurrent stiffening and softening in hydrogels during the dehydration process. Theories based on Flory's work fail to capture the scaling of mechanical behavior with water content, observed in our experiments. We perform coarse-grained molecular dynamics simulations to elucidate the mechanisms underpinning the odd softening-stiffening behavior during dehydration and propose a theoretical model to correctly represent the underlying physics and the divergence from Flory-based theories.

INTRODUCTION

Hydrogels are a class of polymeric materials that contain a large amount of water dispersed within its network. The water content in some hydrogels can even exceed 90%, endowing them the ability to exhibit extremely large deformation (*1*), good biocompatibility (*2*), and excellent ionic and thermal conductivity (*3*, *4*), among other attributes. In response to suitable environmental stimuli (e.g., pH and temperature), the water content in hydrogels can be controllably tuned by dehydration or swelling, and thus, the aforementioned properties can vary across a broad range (*5*–*8*). Accordingly, hydrogels have attracted notable recent attention for applications in intelligent actuating and sensing (*9*–*11*), soft robots (*11*, *12*), stretchable devices (*11*, *13*), artificial tissues, and health care (*14*–*16*). In all these applications, in general, the influence of water content on the basic properties of hydrogels and, specifically, on its mechanical behavior is of significant concern. For example, when applied in stretchable sensing devices and patch material for wound healing as shown in Fig. 1, hydrogels will inevitably lose or absorb water. A widely accepted opinion is that dehydration will stiffen hydrogels (*17*, *18*) and affect the flexibility of hydrogels. Furthermore, the coordination between hydrogels and skin, tissue, or organics may also be altered. However, our results in the present paper prove that this conclusion is questionable. We find that hydrogels can be concurrently stiffened and softened during dehydration due to the concurrent microscopic restrains and relaxations of polymer networks.

Here, we present detailed experiments, complementary molecular dynamics (MD), and theoretical models to understand several key observations pertaining to elastic stiffening and softening of hydrogels and the failure of conventional theories to correctly predict our experiments. On the basis of the insights from our work, through appropriate choice of synthesis conditions, the stiffening and softening effects of hydrogels during dehydration may be controlled, paving the way for many applications for hydrogels as discussed later here.

[1]International Center for Applied Mechanics, State Key Laboratory for Strength and Vibration of Mechanical Structures, Xi'an Jiaotong University, Xi'an 710049, China. [2]Departments of Physics, Materials Science and Engineering and Mechanical Engineering, University of Houston, Houston, TX, USA.
*Corresponding author. Email: zishunliu@xjtu.edu.cn
†These authors contributed equally to this work.

RESULTS

Concurrent mechanical stiffening and softening

An important element for the characterization of mechanical behavior of hydrogels is predicated on extracting the Young's modulus and stress-stretch relation as a function of solvent content. Figure 2 shows our central experimental results for the hydrogel based on polyacrylamide (PAAM) hydrogel. As evident, we note a concurrent mechanical stiffening and softening phenomena during dehydration. Figure 2 (A and B) demonstrates the PAAM hydrogel at its stiff and soft states, respectively, which differ in the ability of deformation. The results in Fig. 2C demonstrate that the Young's modulus of hydrogels increases almost exponentially with the decrease of water content. We label this as "dehydration-induced stiffening phenomenon." Hydrogels with exactly the same water content can show a completely different mechanical behavior (see Fig. 2D), if their as-prepared water content varies. For example, compared with a hydrogel with an as-prepared water content ϕ = 74% (without swelling or dehydration), another hydrogel would be softer if it is dehydrated to ϕ = 74% from a higher, as-prepared water content ϕ' = 83%. We refer to this as the "dehydration-induced softening phenomenon." The stiffening and softening effects both occur during the same dehydration process. Analogously, swelling of hydrogels will lead to similar observations. Figure 2E demonstrates the Young's modulus of PAAM hydrogels with different as-prepared water content and testing water content, in which the concurrent stiffening and softening phenomena can be displayed in a more transparent manner. For the same as-prepared water content, the stiffening effect gets stronger with the increasing of dehydration level. For hydrogels with the same testing water content, the dehydration level increases with an increase in as-prepared water content. Figure 2E shows that the Young' modulus decreases (softening) with an increasing dehydration level when the testing water contents are the same.

Unfortunately, the commonly used Flory-based theories (*19*–*21*) to characterize the mechanical behavior of hydrogels fail to capture the peculiar stiffening and softening phenomena reported in the preceding paragraph. In a now-classical work, Flory and Rehner (*19*) proposed a theoretical model based on statistical thermodynamics to describe the swelling and large deformation behavior of polymers when mixed with a solvent. With the recent focus on research on hydrogels, many researchers have resorted to the direct

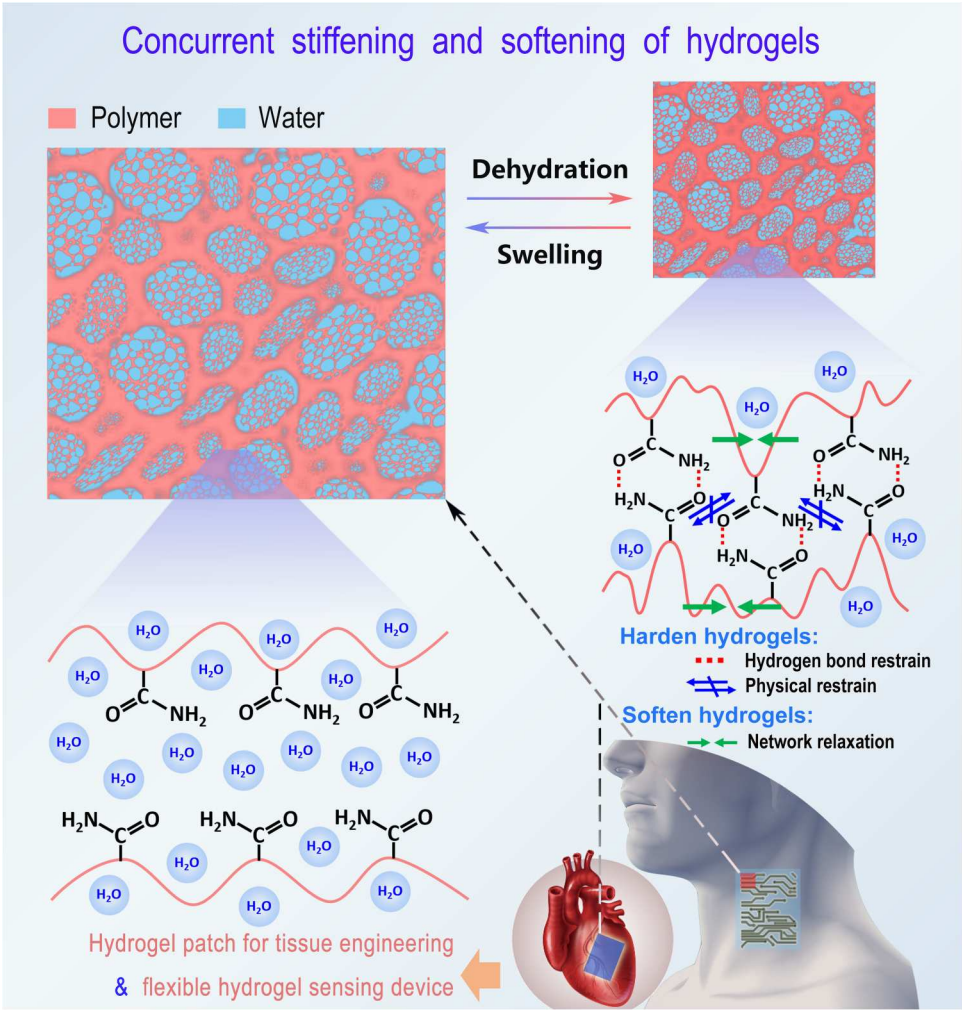

Fig. 1. The concurrent stiffening and softening during dehydration and swelling. The change of water content will induce several aspects of microscopic structural changes of hydrogel concurrently, including hydrogen bond restrain, physical restrain, and network relaxation. The restrains cause the mechanical stiffening effect of hydrogel, while the network relaxation makes the hydrogel softer. By appropriate control of such concurrent stiffening and softening phenomena, applications of hydrogels in many technologies may be facilitated.

(or modified) use of Flory's model to study the mechanical behavior of hydrogels (*8*, *22*–*25*). As we highlight in the following, this can, however, be problematic. Flory-based theories indicate that Young's modulus of hydrogels has a 1/3 power law relationship with water content $[E \propto (1-\phi)^{1/3}]$, which significantly underestimates the stiffening effect during dehydration in Fig. 2E. Meanwhile, Flory-based theories always yield exactly the same mechanical responses regardless of the preparation conditions, thus rendering them unable to predict the dehydration softening effect in Fig. 2D. There are two main reasons that cause the failure of Flory-based theories. The one is that they are completely based on entropic elasticity assumption, which appears to be in contradiction to the molecular-scale restrain effects of polymer chains. Another reason is that Flory's theory was originally proposed to describe the moisture absorption of polymers. The as-prepared state in Flory's theory represents dry polymer networks, while the as-prepared state of hydrogels already contains significant water content. Therefore, it cannot reflect the sensitiveness of mechanical response to the preexisting water content. We further discuss these in the following sections.

We remark that phenomenological constitutive models are also widely used to describe hydrogels (*26*, *27*). This type of models can describe several aspects of the mechanical behavior of hydrogels by fitting appropriate material parameters to experimental results. However, the fitting parameters can deviate significantly between experiments or may even be devoid of any physical meaning. Last, to our knowledge, none of the existing phenomenological models are able to explain the nature of concurrent stiffening and softening phenomenon in hydrogels.

A statistical thermodynamics model

On the basis of a thermodynamics approach, experimental results, and molecular-scale investigations, we attempt to propose a pragmatic (thermodynamics-phenomenological hybrid) theory that can precisely characterize our observations on hydrogels. The details of the derivation can be found in the Supplementary

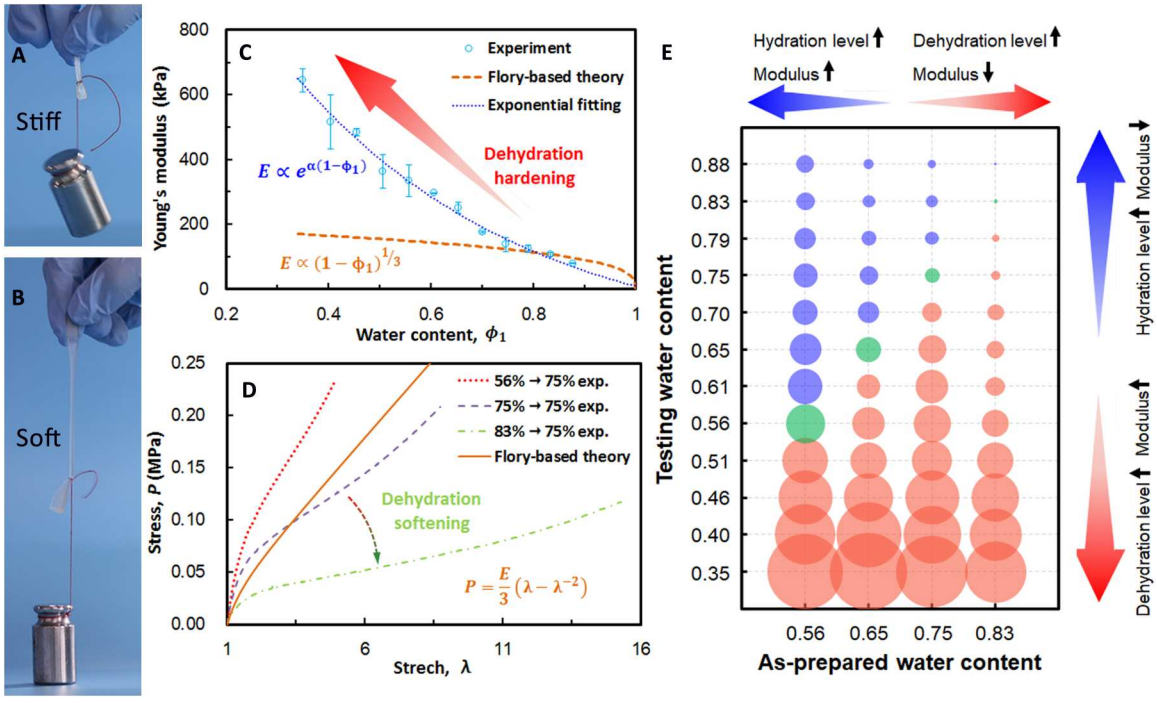

Fig. 2. The mechanical response of PAAM hydrogels. PAAM hydrogel at its (**A**) stiff state and (**B**) soft state. (**C**) Dehydration-induced stiffening effect. The as-prepared water contents are all 75%. With the loss of solvent, Young's modulus of hydrogels increases exponentially. (**D**) Dehydration-induced softening effect. Although the water content during testing is all 75%, a hydrogel would be softer if it has experienced a dehydration process from higher water content. (**E**) Young's modulus of PAAM hydrogels with different as-prepared and testing water content. The red, green, and blue spheres represent that hydrogels are tested at their dehydrated state, as-prepared state, and hydrated state, respectively. The sphere size represents the magnitude of Young's modulus.

Materials (see text S1). Here, we directly give the free-energy density

$$\widehat{W} = \frac{kT}{V_u}\phi_1 \ln\phi_1 - \frac{kT}{V_u}\frac{1-\phi_1}{1-\phi_{10}}\phi_{10}\ln\phi_{10} + \frac{3kT}{2ZV_u}(1-\phi_1) \times \left[(1-\phi_1)^{-\frac{2}{3}} - (1-\phi_{10})^{-\frac{2}{3}}\right] + \frac{\mu}{2}(I_1 - 3) \quad (1)$$

where k is the Boltzmann constant and T is the temperature. ϕ_{10} and ϕ_1 are the volume fractions of the solvent in as-prepared hydrogels and swollen hydrogels, respectively. V_u is the volume of a monomer or solvent molecule, Z is the number of monomers on each polymer chain, $I_1 = \lambda_1^2 + \lambda_2^2 + \lambda_3^2$ is the first invariant of right Cauchy-Green strain tensor, and λ_1, λ_2, and λ_3 are the stretch ratio on three principle directions. μ is the initial shear modulus at small strain written as

$$\mu = \frac{kT}{ZV_u}(1-\phi_1)^{\frac{1}{3}}(1-\phi_{10})^{\frac{2}{3}} \quad (2)$$

We remark that there are two water content identities in the expression of our free-energy density, i.e., the as-prepared water content ϕ_{10} and the current water content ϕ_1 after a swelling or dehydration process. We can see that if $\phi_{10} = 0$ (as-prepared water content is 0), Eqs. 1 and 2 will exactly reduce to the well-known Flory's form (*19*, *28*). This is because the reference state in Flory's theory is a dry polymer network, and it is originally proposed to describe the hydration swelling and deformation of polymers. Thus, the naive use of Flory's theory is ill-advised because of the presence of a large amount of preexisting water content in as-prepared hydrogels.

Our theory is suitable to characterize the sensitivity of hydrogels' mechanical properties to the preparation conditions as shown in Fig. 2D. Because of the incompressibility assumption, we have $\lambda_1 = \lambda$, $\lambda_2 = \lambda_3 = \lambda^{-0.5}$ for the uniaxial tension situation. Here, λ is the stretch on the uniaxial tension direction. Defining nominal stress as the work conjugate to the stretch λ, we have the nominal stress

$$P_1 = \mu(\lambda - \lambda^{-2}) \quad (3)$$

For the same testing water content ϕ_1, Eq. 3 will yield a smaller nominal stress if the as-prepared water content ϕ_{10} is higher, which is consistent with our experiments as shown in Fig. 2D. Then, the Young's modulus is $E = \frac{\partial P_1}{\partial \lambda}|_{\lambda=1} = 3\mu$, which is valid for incompressible materials.

Dehydration-induced network restraints and mechanical stiffening

The free-energy density in Eq. 1 is still completely based on entropic elasticity hypothesis, which assumes that the free energy is dominated by the configurational entropy of networks, without considering the interactions between these networks. As a result, the modulus in Eq. 2 retains the 1/3 power law relationship with water content ϕ_1, thus unable to correctly describe the marked stiffening phenomenon in Fig. 2E. However, the real network chains will inevitably interact with their neighbors through friction, hydrogen bond restraints, and entanglements. Here, we use coarse-grained molecular dynamics (CGMD) to investigate the influence of such

microscopic interactions on chains' activity and mechanical response of hydrogels.

Hydrogels are composed of cross-linked networks and water with a random configuration. In the present paper, we construct such molecular models of PAAM hydrogel by a reaction method. The details of our molecular modeling method can be found in Materials and Methods. The final randomly cross-linked PAAM hydrogel model with an initial water content of 72% is displayed in Fig. 3. By randomly deleting solvent particles from the system, we can obtain dehydrated hydrogels. Similarly, we obtain the swollen hydrogels by adding solvent.

For hydrogels with varying water content, the diffusion coefficient D_c of polymer network particles, which characterizes the mobility of polymer chains, is investigated by CGMD simulations. As shown in Fig. 4A, the diffusivity of polymer particles decreases markedly with the dehydration of hydrogels. The diffusion trajectories of polymer particles within 100 ps are also recorded during the simulations as shown in Fig. 4A. We define the minimum circumscribed circle (MCC) of a particle's trajectory as its diffusion zone and the radius of MCC as its diffusion radius r_d. For each water content, r_d is averaged over 500 particles. From Fig. 4B, we can see that the diffusion zone of polymer would be bigger when water content increases, i.e., when water acts as lubricant and reduces the restraint between polymer networks. Sekine and Ikeda-Fukazawa (*29*) have studied the structural change of water in a hydrogel during dehydration. They find that the residual water forms a hydrogen-bond network when water content is low, which may restrain the motion of polymer networks. We also calculated the radical distribution function (RDF) of polymer molecules in PAAM hydrogels. As shown in Fig. 4C, we define the radius of first peak on RDF as R_p, which represents the distance of polymer molecules to their neighbors. With a smaller neighbors distance R_p, the polymer molecules will be more likely to restrain each other. Figure 4B shows that R_p increases with the increasing of water content.

We use attenuated total reflection Fourier transform infrared spectroscopy (ATR/FTIR) analysis to measure the polymer chain density on hydrogel surfaces. As shown in Fig. 4D, PAAM hydrogels show significant peaks at ~1605 cm^{-1} (N—H bending) and ~1652 cm^{-1} (C═O stretching) (*30*, *31*). The absorbance reduces with increasing water content, suggesting that the increasing of water content results in decreasing of surface chain density. The RDF and ATR/FTIR results also confirm that water molecules will separate polymer networks and decrease the restraint effect between them. Here, we define another parameter $R_s = 1/D_c$ to measure the restraint level between polymer chains. As displayed in Fig. 4E, the restraint effect will be reinforced exponentially ($R_s \propto e^{-\alpha\phi_1}$) with the dehydration of hydrogels. The diagrams in Fig. 4E explain the stiffening mechanism. When water content is high, the polymer chains are dispersed and the interactions between them are weak. As the dehydration and shrinking of hydrogel proceeds, chains engage and restrain each other by van der Waals interactions, hydrogen bonds, intermolecular frictions, and entanglements. Consequently, the activity of chains is reduced, making the networks stiffer. Hence, we consider such exponential stiffening effect into our theoretical constitutive model by introducing an exponential multiplier, namely

$$\mu = \frac{kT}{\eta Z V_u} e^{-\alpha\phi_1} (1-\phi_1)^{\frac{1}{3}} (1-\phi_{10})^{\frac{2}{3}} \quad (4)$$

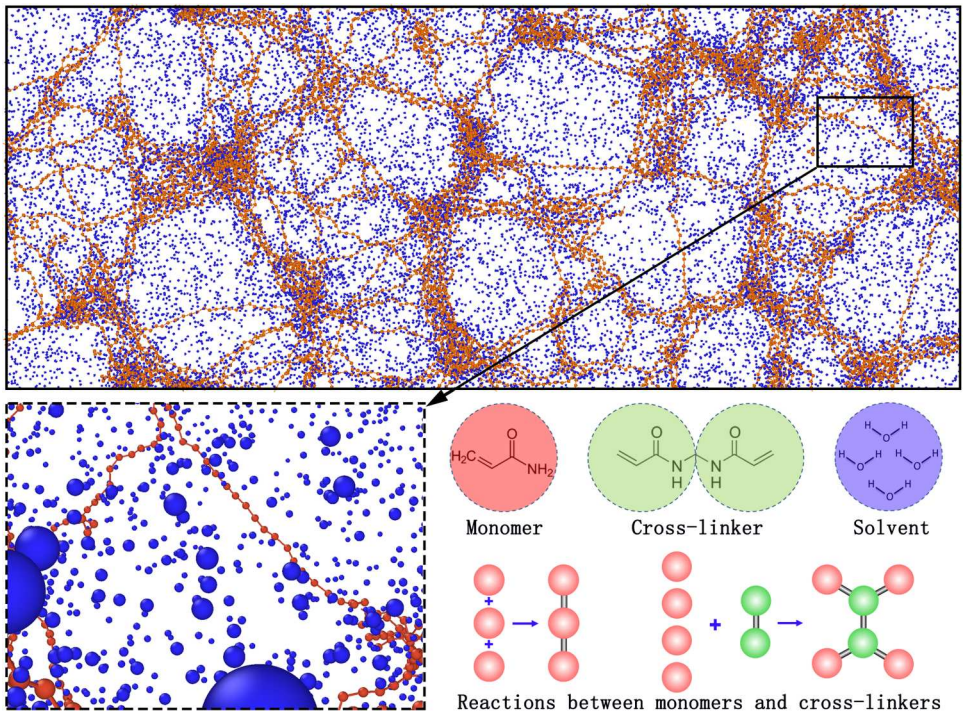

Fig. 3. The CGMD model. The PAAM hydrogel model is generated by a reaction method. A monomer and four water molecules are regarded as one particle, while a cross-linker is regarded as two connected particles.

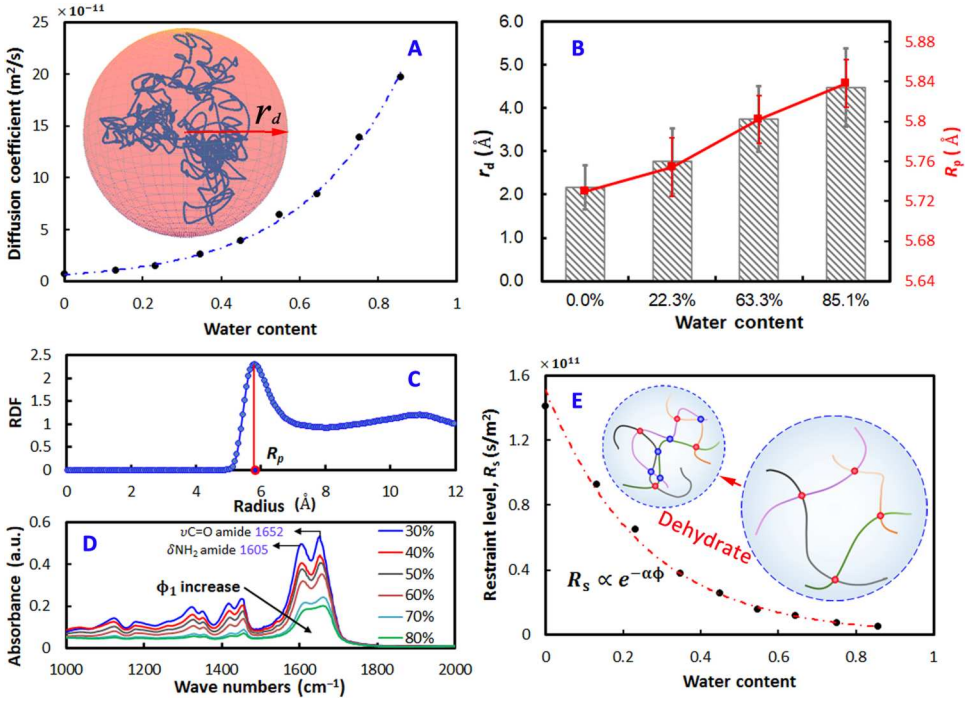

Fig. 4. Microscopic transition during dehydration. (**A**) Diffusion coefficient of polymer molecules in hydrogels with different water contents. The red sphere represents the diffusion trajectory and diffusion zone of a monomer on PAAM chains. (**B**) Averaged diffusion radius and RDF of polymer molecules in hydrogels with different water contents. (**C**) RDF of polymer molecules in PAAM hydrogels; the water content is 53.47%. (**D**) ATR/FTIR absorption spectra of PAAM hydrogels. (**E**) Restraint levels between polymer molecules. Dehydration will enhance the restraint levels exponentially. The blue dots represent the binding points between polymer chains introduced by dehydration.

The microscopic binding between chains can be equivalently regarded as introducing extra cross-linking points (the blue dots in Fig. 4E) into networks. Therefore, we accordingly introduce a correction factor η to Z (monomer number between cross-linkages), which satisfies $0 < \eta < 1$.

To validate our theoretical model, we have compared our model with experiments. We first prepared PAAM hydrogels with different initial water contents, while the mass ratio between monomer and cross-linker ($R_{m\text{-}c}$) is kept as 1000:1. These as-prepared hydrogels are then dehydrated or swelled to different water contents and cut into bone-shaped specimens. Uniaxial tension experiments were carried out on these hydrogel specimens. Figure 5 shows the Young's modulus of hydrogels with different as-prepared and testing water contents. As shown in Fig. 5, our theoretical model can precisely capture the stiffening phenomenon and agrees well with our experiments. We also carried out experiments by changing the cross-linking density, i.e., $R_{m\text{-}c}$ = 10,000:1 and $R_{m\text{-}c}$ = 100:1. Similar results are obtained, and our theory agrees well with them all (see text S2).

Dehydration softening: Entanglements and dehydration-induced network relaxation

The constitutive model in Eq. 3 can predict the dehydration softening behavior of hydrogels. For the same testing water content ϕ_1, Eq. 3 will give a smaller nominal stress if the prepared water content ϕ_{10} is higher, which is consistent with our experiments as shown in Fig. 2D. By using MD simulations, we have compared the diffusion abilities of two sets of hydrogel networks whose water contents are both 53%. Hydrogels in the first set are in their as-prepared states, while hydrogels in the second set are dehydrated from water content 74%. As shown in Fig. 6A, the diffusion coefficient and diffusion radius of networks in the first set are both smaller than those in the second set, which indicates that the polymer networks in the second set have stronger motion ability and are thus softer. This is consistent with our experimental results, i.e., dehydration softening effect. An important reason for this observation is that the entanglement is stronger when as-prepared water content is low, as pointed out in Kim *et al.*'s paper (*32*, *33*). These entanglements will restrain the motion ability of networks. According to Kim *et al.*, the cross-linking density (mass ratio between monomer and cross-linker, $R_{m\text{-}c}$) would also affect the entanglement level. We have carried out our experiments on three cross-linking densities, i.e., $R_{m\text{-}c}$ = 10,000, 1000, and 100, respectively, and the entanglements will cover from super large to very low. However, the dehydration softening effect always exists. Therefore, there must be some mechanisms more behind this phenomenon. We think another reason for this observation is that hydrogels in the second set have experienced a dehydration process, which introduces a pre-relaxation to the networks and increases their mobility as displayed in Fig. 6B. When dehydrated to the same testing water content, the pre-relaxation effect will be more obvious if the initial water content is higher. Consequently, the second set of hydrogels is easier to deform, i.e., are softer.

The hyperelastic behavior of soft materials is usually characterized by the free energy of deformation, in which the initial modulus μ is a key parameter. Researchers have proposed many famous

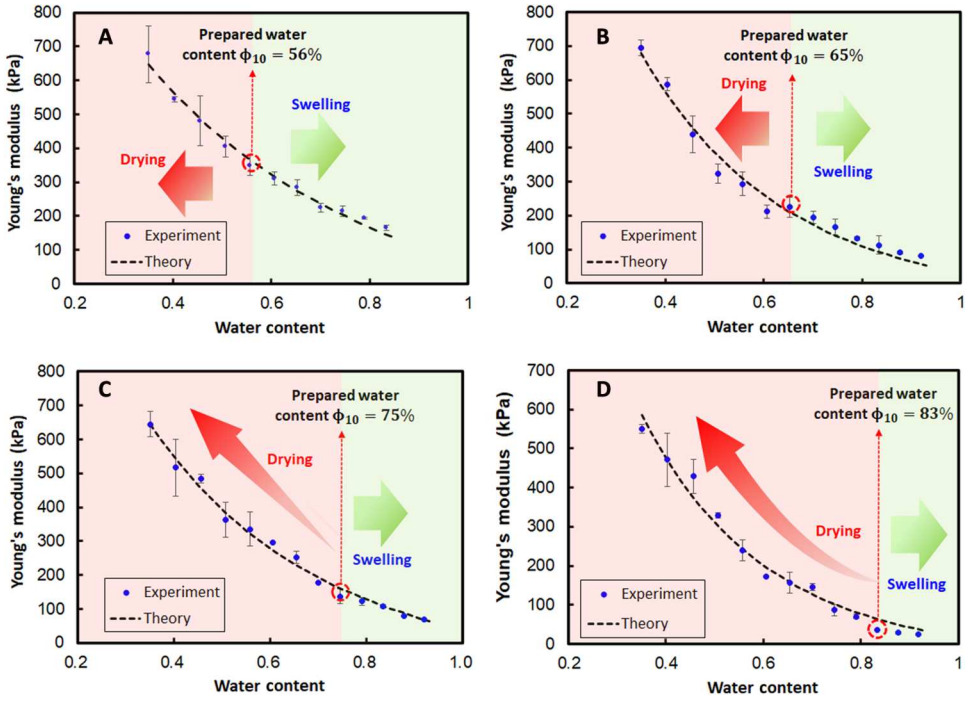

Fig. 5. The stiffening effect: Comparison between experiment and theory. The as-prepared water contents are (**A**) 56%, (**B**) 65%, (**C**) 75%, and (**D**) 83%, respectively.

hyperelastic models. For example, the stretching-induced free energy term in Eq. 1 is of neo-Hookean form, i.e., $\widehat{W}_{str} = \mu(I_1 - 3)/2$. However, when we substitute the real shear modulus μ into these models, we are unable to obtain the correct stress-stretch relationship for hydrogels. As shown in Fig. 6C, hydrogels first experience a serious softening stage with the uniaxial tension process, which is followed by a stiffening period at super large deformation. Although the neo-Hookean model also contains a softening stage, it still highly overestimates the nominal stress of hydrogels. In addition, the neo-Hookean model can never predict the stiffening behavior at large deformations. Many constitutive models have been proposed to characterize the stiffening phenomenon of polymer materials, such as the Gent model (Eq. 5) (*26*, *34*) and the exponential neo-Hookean model (Eq. 6) (*35*)

$$\widehat{W}_{\mathrm{G}} = \frac{\mu}{2} J_{\mathrm{m}} \ln\left(1 - \frac{I_1 - 3}{J_m}\right), J_{\mathrm{m}} > I_1 - 3 \tag{5}$$

$$\widehat{W}_{\mathrm{E}} = \frac{\mu}{2} I_c (e^{\frac{I_1 - 3}{I_c}} - 1), I_c > 0 \tag{6}$$

where J_{m} represents the limiting extensibility of materials and I_{c} is a characteristic strain for stiffening behavior to occur. These two models both reduce to the classical neo-Hookean model in the small strain regime, for example, taking $J_{\mathrm{m}} \to \infty$ and $I_{\mathrm{c}} \to \infty$. Therefore, these models still highly overestimate the stress level of hydrogels as shown in Fig. 6C. This conclusion is also valid for the well-known Arruda-Boyce model (*36*); hence, we do not belabor this point further.

The Mooney-Rivlin model (*37*) can well capture the strain softening behavior by introducing the second invariant $I_2 = \lambda_1^2\lambda_2^2 + \lambda_2^2\lambda_3^2 + \lambda_3^2\lambda_1^2$ into the free energy

$$\widehat{W}_{\mathrm{MR}} = \frac{\mu}{2}[\omega(I_1 - 3) + (1 - \omega)(I_2 - 3)] \tag{7}$$

where ω is a weight coefficient to distribute the first and second invariant terms. ω should satisfy the condition $0 \le \omega \le 1$ to maintain $E = 3\mu$. Equation 7 reduces to the neo-Hookean model when ω = 1. As shown in Fig. 6C, the Mooney-Rivlin model can be regarded as a softened neo-Hookean model and thus can possibly characterize the strain softening behavior of hydrogels, although the stiffening phenomenon at large deformations is still elusive.

The above discussions encourage us to rewrite our stretching free energy in Eq. 1 by introducing I_2-related terms into a stiffened neo-Hookean model. For example, we propose the following free energy with the exponential neo-Hookean model used to characterize the strain stiffening effect

$$\widehat{W}_{\mathrm{str}} = \frac{\mu}{2}[\omega I_{1c}(e^{\frac{I_1 - 3}{I_{1c}}} - 1) + (1 - \omega)(I_2 - 3)] \tag{8}$$

The expression of μ is given in Eq. 4, and the inequality $0 \le \omega \le 1$ should also be satisfied. When the parameter $I_{1c} \to \infty$, this model will reduce to the Mooney-Rivlin model, and additionally, if ω = 1 is satisfied, our model will reduce to the neo-Hookean model (our previously deduced form in Eq. 1). From Fig. 6C, we can see that our model can precisely capture the strain softening behavior in median strain region and the strain stiffening behavior at very large deformations. Significantly, the expression in Eq. 8 is only one of the many optional forms of our free energy. We may also alternatively use other expressions by replacing the two terms in Eq. 8, and they all perform extremely well when predicting the super large deformation behavior of hydrogels as shown in fig. S7 (see text S3).

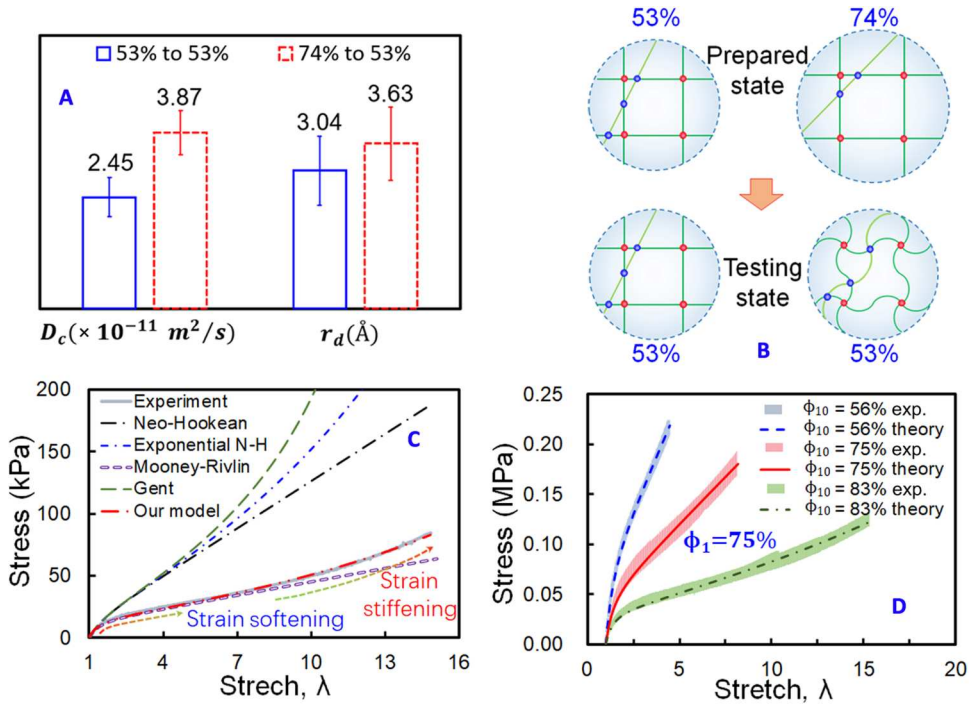

Fig. 6. Dehydration-induced softening. (**A**) Diffusion coefficient and diffusion radius of polymer molecules in two hydrogels whose water contents are both 53%. But one is as-prepared, while the other one is dehydrated from 74% water contents. (**B**) Sketch of the configurations of these two types of hydrogels. The blue dots represent the entanglements and restraints between polymer chains. (**C**) Comparison of uniaxial tension results between different theoretical models and experiments. (**D**) Results of our model and experiments. The testing water contents are all 75%, while their as-prepared water content varies.

We prepared three sets of hydrogel specimens whose initial water contents are ϕ_{10} = 56%, ϕ_{10} = 75%, and ϕ_{10} = 83%, respectively, while the mass ratio between monomer and cross-linker is 1000:1. These three sets of specimens with different ϕ_{10} are all dehydrated or swelled to a testing water content of ϕ_1 = 75%, after which uniaxial tension tests are carried out on these specimens. For each hydrogel set, at least three specimens are tested and the strips in Fig. 6D display the distributions of their stress-stretch curves. Just as we have discussed in the preceding paragraphs, for the same water contents, a hydrogel is softer if it has undergone a dehydration process from a higher prepared water content. We call it the dehydration softening phenomenon. On the other hand, the hydrogel would be harder if it has been swelled from a lower water content. As demonstrated in Fig. 6D, our theoretical model can precisely capture such sensitiveness phenomenon of mechanical response of hydrogels based on its preparation conditions. The validation of our theory is confirmed based on tension experiments of hydrogels with other testing water contents and cross-linking densities (see text S2).

On the basis of our experimental findings, we proposed several application scenarios, including intelligent actuating devices and modeling of the growth of plants, as shown in fig. S8. In our designs, the structures are all composed of a matrix and some ribs with special arranged configurations. In the initial state of our structures (fig. S8, A1 to C1), the water contents ϕ_1 as well as the chemical potential $\overline{\omega}/kT$ in the matrix and ribs are the same, whereas their as-prepared water contents ϕ_{10} differ. Figure S8D shows the detailed structures of our designs. When subjected to water environment, the matrix and ribs will get hydrated under the driving of chemical potential difference between the structures and environment. The original homogeneously distributed water content will diverge to two different evolution directions as displayed in fig. S8E. After the structures get equilibrated with the environment ($\overline{\omega}/kT$ = 0), the water contents in the matrix and ribs will be quite different. The matrix will absorb more water and be soft, while the ribs are less hydrated and be relatively stiff. Because of the swelling ratio and stiffness mismatch, the structures then get deformed. As a result, structures A, B, and C are twisted, scrolled, and wrinkled, respectively. Figure S8 (A2 to A5) displays the side view along the major axis. These results are obtained by implanting our theory into COMSOL software [see the finite element method (FEM) simulation part in Materials and Methods]. Structures A and B may be used as underwater actuating devices, which perform rotating and grabbing functions, respectively. By appropriate programming of these deformations, we are able to obtain soft robots with more complex functions. Structure C may be used to explain the growth and morphology evolution of lotus leaf. With specific choice of the structural designs, we can also model and reproduce the growth of diverse living beings.

DISCUSSION

Our experimental results demonstrate that hydrogels exhibit concurrent mechanical stiffening and softening during dehydration. The Young's modulus of hydrogels increases almost exponentially with the decrease of water content in hydrogels, i.e., dehydration-induced mechanical stiffening. However, the most widely used Flory's theory and existing theories based on Flory's work to

characterize hydrogels' mechanical behavior indicate that Young's modulus has a 1/3 power law relationship with water content. The reason for the failure of Flory-based theories to predict the stiffening effect is that they are based entirely on entropic elasticity. This is in contrast to our atomistic simulations, which provide clear evidence that solely relying on entropic elasticity for the hydration or dehydration of hydrogels is ill-justified. Our atomistic simulations demonstrate that the polymer chains would be bound and that their mobility would decrease gradually during the dehydration of hydrogels. Therefore, the entropic elasticity assumption is not valid anymore. On the other hand, for the same testing water content, a hydrogel would be softer if it has experienced a dehydration process from an as-prepared state with higher initial water content. We call this the dehydration-induced softening phenomenon of hydrogels. However, the existing theories always give exactly the same mechanical response no matter what preparing condition it is. Our molecular-scale investigation reveals that dehydration would introduce a pre-relaxation of polymer chains and increase the mobility and, as a result, make the hydrogel softer. Meanwhile, there would be more entanglements in the networks if as-prepared water content is low and makes the gel stiffer. Thus, the dehydration softening effect is induced by both the pre-relaxation and entanglement level difference in gels. On the basis of our experiments and molecular-scale investigations, we have proposed a statistical thermodynamics-based phenomenological theory that is able to precisely capture the phenomena of concurrent stiffening and softening for hydrogels during dehydration.

The opportunities for the application of this approach to existing problems in soft robotics, self-assembly, and explaining the fundamental mechanisms in polymer physics and morphology evolution of plants are vast. A first example here is four-dimensional printing of functional flexible structures. By printing polymer gels with different as-prepared water contents at specific positions of an as-printed structure, we can obtain other complex structures after time-dependent stimuli (dehydration or hydration). This morphology transition or self-assembly of printed structures is enabled by the stiffness difference and swelling mismatch between different regions. Further interest is expected in the field of intelligent actuators and robots responding to the environmental stimuli. Figure S8 has shown the application of our findings in the underwater arms that can perform grabbing and twisting actions. By manufacturing more detailed structures, we are able to realize more complex functions, such as designing artificial fishes and flexible robots, manufacturing pasta, and modeling the growth of plants. Another significance of this approach lies in revealing the nature of atomic-level chain interaction patterns and the role of solvents played between them in polymers and polymer gels. It may also be useful for the design of polymeric materials.

MATERIALS AND METHODS

Materials preparation

In the present research, a light curing method is adopted for the synthesis of PAAM hydrogel as shown in fig. S9. In this method, acrylamide (AAM; monomer) is mixed up with *N*,*N*′-methylenebisacrylamide (MBAA; the cross-linker) and 2-hydroxy-4′-(2-hydroxyethoxy)-2-methylpropiophenone (Irgacure 2959; the curing agent) with a mass ratio of 1000:1:10. Then, the powder mixture is dissolved into deionized water and stirred for at least 6 hours. By tuning the mass ratio of powder mixture and water, we can have solutions with different water contents. In the present research, we prepared four sets of solutions whose water contents (mass fraction) are 50, 60, 70, and 80%, respectively. Because we use the volume fraction as the water content in our theory, we convert the mass friction into volume friction by the following relationship

$$\phi_1 = \frac{\rho_2 F_1}{\rho_1(1 - F_1) + \rho_2 F_1} \tag{9}$$

where F_1 is the mass fraction of water in hydrogels and $\rho_1 = 1.0000$ g/cm^3 and $\rho_2 = 1.2575$ g/cm^3 are the mass densities of water and dry PAAM networks, respectively. The solutions are then injected into a mold (150 mm × 150 mm × 2 mm) and subjected to ultraviolet light environment to conduct the curing process for another 6 hours.

Mechanical tests

The cured PAAM hydrogels are cut into as-prepared specimens as shown in fig. S9C. The as-prepared specimens are subjected to natural evaporation or deionized water to get dehydrated or swollen specimens with specific water contents. Then, the dehydrated or swollen specimens are sealed into plastic bags for at least 4 hours to obtain uniform water distributions. We seal the specimen for about 4 hours only when the water content change is very small, for example, from 70% to 60%. When the water content change is large, we have sealed them for at least 1 day. We have also confirmed this by comparing the modulus of specimens that sealed for different time. As shown in fig. S10, it is enough for the modulus to reach a constant value after 1 day. In addition, for most of the cases, 2 hours is enough, although the water content change is large. For the results displayed in figs. S5 and S6, all of the specimens are sealed for 4 days. Last, we have the testing specimens with various water contents and carry out uniaxial tension tests using these specimens. Because PAAM hydrogel can easily lose its water when exposed into air, the specimens are kept in a steam chamber during tension tests as shown in fig. S9F to maintain the water content in the hydrogel specimens and their mechanical properties. The uniaxial tension tests are carried out on the tensile machine (Shimadzu AGS-X). A small loading speed (10 mm/min) is adopted to obtain a quasi-static loading situation. Before and after tests, the weight of specimens is measured to make sure that the water content change is less than 3% during the long time tension. The size of specimens before tests is also recorded to calculate the nominal stress and stretch. A typical stress-stretch curve of PAAM hydrogel is displayed in fig. S9D. It consists of a softening stage at small and medium strain and a stiffening stage at super large deformation. In hyperelastic theories, the initial modulus at small strain is a key parameter to characterize the mechanical behavior of materials. We determine the initial modulus of PAAM hydrogel by linearly fitting the stress-stretch curve within a 5% strain as shown in fig. S11D.

ATR/FTIR tests

Functional groups in materials can absorb infrared ray (IR) if the IR frequency is equal to the vibration frequency of functional groups. For example, the bending wave number of N—H (amide) and the stretching wave number of C═O (amide) are 1605 cm^{-1} and ~1652 cm^{-1}, respectively (*29*, *30*). The absorptance of IR can

reflect the functional group density in materials, i.e., higher absorptance peek means higher group density. In the present paper, we use ATR/FTIR analysis (test on Thermo Fisher Scientific Nicolet iS50 machine) to measure the absorption spectra of PAAM hydrogel. PAAM hydrogels with solvent contents of 30, 40, 50, 60, 70, and 80% are tested.

CGMD model

In the modeling method, a single AAM monomer is regarded as one particle, while an MBAA (the cross-linker) molecule is set as two connected particles with a covalent bond as shown in Fig. 3. Besides, one solvent particle consists of four H_2O molecules. The monomer, cross-linker, and solvent particles are mixed randomly with a molar ratio of 800:1:2000, resulting in a water mass fraction of about 72%. As displayed in Fig. 3, there are C═C bonds in monomers and cross-linkers. In the real cross-linking reactions, these C═C bonds will turn into C–C bonds and connect to other monomers or cross-linkers and form a cross-linked structure. In our modeling process, the mixture of particles is subjected to random thermal diffusion under the isothermal-isobaric ensemble while using Martini force field (*38*) to describe the interactions between particles. During the diffusion, a covalent bond would be added between two monomers or cross-linker particles if their distance is less than 0.45 nm. Just like real reactions, the maximum number of particles that each monomer or cross-linker particle can connect is 2. Because each MBAA contains two particles, a cross-linker can connect four monomers. This reaction process is performed in large-scale atomic/molecular massively parallel simulator (LAMMPS) until most of the monomers and cross-linkers are connected. The final PAAM hydrogel model with a water content of 72% is displayed in Fig. 3. The morphology of our model is quite similar with real structures of hydrogels (*1*, *39*). Besides, the average density of the PAAM hydrogel we measured in the laboratory is 1.0300 ± 0.0190 g/cm^3 when the water mass fraction is between 40 and 70% (*4*), which is almost the same as our CGMD models (1.0117 ± 0.0133 g/cm^3).

FEM simulation

We build the models in fig. S8 using the FEM software COMSOL and implant the constitutive model in Eq. 1 into it. By calculating the partial derivative of free-energy density with water content, we have the chemical potential of water molecules in hydrogels, namely

$$\frac{\overline{\omega}}{kT} = \frac{1}{kT}\frac{\partial \widehat{W}}{\partial \phi_1} \tag{10}$$

The chemical potential is always a negative number, while the potential of pure water is 0. When subjected to water environment, the structures in fig. S8 will absorb water and swell under the driving force of potential gradient. In addition, the diffusion of water is governed by

$$J = -D\nabla\frac{\overline{\omega}}{kT} \tag{11}$$

where D is the diffusion coefficient of water. After the chemical potential increases to 0, the structures will get fully swelled and we have the equilibrium structures in fig. S8 (A5, B5, and C6). The as-prepared water content ϕ_{10} in the matrix and ribs are 0.8 and 0.6, respectively.

Supplementary Materials

This PDF file includes:

Supplementary Text
Figs. S1 to S11
References

REFERENCES AND NOTES

1. K. Cui, T. L. Sun, X. Liang, K. Nakajima, Y. N. Ye, L. Chen, T. Kurokawa, J. P. Gong, Multiscale energy dissipation mechanism in tough and self-healing hydrogels. *Phys. Rev. Lett.* **121**, 185501 (2018).
2. F. Campos, A. B. Bonhome-Espinosa, J. Chato-Astrain, D. Sánchez-Porras, I. A. Rodriguez, Evaluation of fibrin-agarose tissue-like hydrogels biocompatibility for tissue engineering applications. *Front. Bioeng. Biotechnol.* **16**, 596 (2020).
3. C. H. Yang, B. Chen, J. J. Lu, J. H. Yang, J. Zhou, Y. M. Chen, Z. Suo, Ionic cable. *Extreme Mech. Lett.* **3**, 59–65 (2015).
4. S. Xu, S. Cai, Z. Liu, Thermal conductivity of polyacrylamide hydrogels at the nanoscale. *ACS Appl. Mater. Interfaces* **10**, 36352–36360 (2018).
5. Z. Ding, W. Toh, J. Hu, Z. Liu, Y. N. Teng, A simplified coupled thermo-mechanical model for the transient analysis of temperature-sensitive hydrogels. *Mech. Mater.* **97**, 212–227 (2016).
6. A. D. Drozdov, J. D. Christiansen, Swelling of pH-sensitive hydrogels. *Phys. Rev. E* **91**, 022305 (2015).
7. S. Xu, Z. Liu, A nonequilibrium thermodynamics approach to the transient properties of hydrogels. *J. Mech. Phys. Solids* **127**, 94–110 (2019).
8. R. Huang, S. Zheng, Z. Liu, T. Y. Ng, Recent advances of the constitutive models of smart materials—Hydrogels and shape memory polymers. *Int. J. Appl. Mech.* **12**, 2050014 (2020).
9. C. Xuan, Y. Zhou, Y. Zhao, X. He, L. Jin, Photodriven self-excited hydrogel oscillators. *Phys. Rev. Appl.* **17**, 014007 (2022).
10. J. Guo, X. Liu, N. Jiang, A. K. Yetisen, H. Yuk, C. Yang, A. Khademhosseini, X. Zhao, S. H. Yun, Highly stretchable, strain sensing hydrogel optical fibers. *Adv. Mater.* **28**, 10244–10249 (2016).
11. X. Liu, J. Liu, S. Lin, X. Zhao, Hydrogel machines. *Mater. Today* **36**, 102–124 (2020).
12. Y. Kim, H. Yuk, R. Zhao, S. A. Chester, X. Zhao, Printing ferromagnetic domains for untethered fast-transforming soft materials. *Nature* **558**, 274–279 (2018).
13. H. Yuk, B. Lu, S. Lin, K. Qu, X. Zhao, 3D printing of conducting polymers. *Nat. Commun.* **11**, 1604 (2020).
14. X. Chen, H. Yuk, J. Wu, C. S. Nabzdyk, X. Zhao, Instant tough bioadhesive with triggerable benign detachment. *Proc. Natl. Acad. Sci. U.S.A.* **117**, 15497–15503 (2020).
15. C. Keplinger, J. Y. Sun, C. C. Foo, P. Rothemund, G. M. Whitesides, Z. Suo, Stretchable, transparent, ionic conductors. *Science* **341**, 984–987 (2013).
16. R. Contreras-Cáceres, M. C. Leiva, R. Ortiz, A. Díaz, G. Perazzoli, M. A. Casado-Rodríguez, C. Melguizo, J. M. Baeyens, J. M. López-Romero, J. Prados, Paclitaxel-loaded hollow-poly(4-vinylpyridine) nanoparticles enhance drug chemotherapeutic efficacy in lung and breast cancer cell lines. *Nano Res.* **10**, 856–875 (2017).
17. E. Zhang, R. Bai, X. P. Morelle, Z. Suo, Fatigue fracture of nearly elastic hydrogels. *Soft Matter* **14**, 3563–3571 (2018).
18. Z. Q. Li, Z. S. Liu, T. Y. Ng, P. Sharma, The effect of water content on the elastic modulus and fracture energy of hydrogel. *Extreme Mech. Lett.* **35**, 100617 (2020).
19. P. J. Flory, J. Rehner Jr., Statistical mechanics of cross-linked polymer networks II. Swelling. *J. Chem. Phys.* **11**, 521–526 (1943).
20. W. Hong, X. Zhao, J. Zhou, Z. Suo, A theory of coupled diffusion and large deformation in polymeric gels. *J. Mech. Phys. Solids* **56**, 1779–1793 (2008).
21. Z. Liu, W. Toh, T. Y. Ng, Advances in mechanics of soft materials: A review of large deformation behavior of hydrogels. *Int. J. Appl. Mech.* **7**, 1530001 (2015).
22. S. Xu, Z. S. Liu, Coupled theory for transient responses of conductive hydrogels with multi-stimuli. *J. Mech. Phys. Solids* **143**, 104055 (2020).
23. W. Hong, Z. S. Liu, Z. G. Suo, Inhomogeneous swelling of a gel in equilibrium with a solvent and mechanical load. *Int. J. Solids Struct.* **46**, 3282–3289 (2009).
24. R. Xiao, J. Qian, S. X. Qu, Modeling gel swelling in binary solvents: A thermodynamic approach to explaining cosolvency and cononsolvency effects. *Int. J. Appl. Mech.* **11**, 1950050 (2019).
25. T. Bertrand, J. Peixinho, S. Mukhopadhyay, C. W. Macminn, Dynamics of swelling and drying in a spherical gel. *Phys. Rev. Appl.* **6**, 064010 (2016).
26. V. Manish, A. Arockiarajan, G. Tamadapu, Influence of water content on the mechanical behavior of gelatin based hydrogels: Synthesis, characterization, and modeling. *Int. J. Solids Struct.* **233**, 111219 (2021).
27. Y. Mao, S. Lin, X. Zhao, L. Anand, A large deformation viscoelastic model for double-network hydrogels. *J. Mech. Phys. Solids* **100**, 103–130 (2017).

28. P. J. Flory, *Principles of Polymer Chemistry* (Cornell Univ. Press, 1953).
29. Y. Sekine, T. Ikeda-Fukazawa, Structural changes of water in a hydrogel during dehydration. *J. Chem. Phys.* **130**, 034501 (2009).
30. Z. D. Zhou, J. C. Lei, Z. S. Liu, Effect of water content on physical adhesion of polyacrylamide hydrogels. *Polymer* **246**, 124730 (2022).
31. O. O. Oyeneye, W. Z. Xu, P. A. Charpentier, Adhesive RAFT agents for controlled polymerization of acrylamide: Effect of catechol-end R groups. *RSC Adv.* **5**, 76919–76926 (2015).
32. J. Kim, G. Zhang, M. Shi, Z. Suo, Fracture, fatigue, and friction of polymers in which entanglements greatly outnumber cross-links. *Science* **374**, 212–216 (2021).
33. Y. Wang, G. Nian, J. Kim, Z. Suo, Polyacrylamide hydrogels. VI., Polyacrylamide hydrogels. VI. Synthesis-property relation. *J. Mech. Phys. Solids* **170**, 105099 (2023).
34. A. N. Gent, A new constitutive relation for rubber. *Chem. Technol.* **69**, 59–61 (2012).
35. J. Lin, S. Y. Zheng, R. Xiao, J. Yin, J. Qian, Constitutive behaviors of tough physical hydrogels with dynamic metal-coordinated bonds. *J. Mech. Phys. Solids* **139**, 103935 (2020).
36. E. M. Arruda, M. C. Boyce, A three-dimensional constitutive model for the large stretch behavior of rubber elastic materials. *J. Mech. Phys. Solids* **41**, 389–412 (1993).
37. M. Mooney, A theory of large elastic deformation. *J. Appl. Phys.* **11**, 582–592 (1940).
38. S. J. Marrink, H. J. Risselada, S. Yefimov, D. P. Tieleman, A. D. Vries, The MARTINI force field: Coarse grained model for biomolecular simulations. *J. Phys. Chem. B* **111**, 7812–7824 (2007).
39. H. C. G. De Cagny, B. E. Vos, M. Vahabi, N. A. Kurniawan, M. Doi, G. H. Koenderink, F. C. Mackintosh, D. Bonn, Porosity governs normal stresses in polymer gels. *Phys. Rev. Lett.* **117**, 217802 (2016).
40. P. J. Flory, J. Rehner, Statistical mechanics of cross-linked polymer networks. I. Rubberlike elasticity. *J. Chem. Phys.* **11**, 512–520 (1943).

Acknowledgments

Funding: This work was funded by National Natural Science Foundation of China grants 11820101001, 12102330, and 12172273 and China Postdoctoral Science Foundation grant 2021M690125. **Author contributions:** Conceptualization: S.X. and Z.L. Methodology: S.X. and Z.Z. Investigation: S.X. and Z.Z. Visualization: S.X. and Z.Z. Supervision: Z.L. and P.S. Writing—original draft: S.X. Writing—review and editing: S.X., Z.Z., Z.L., and P.S. **Competing interests:** The authors declare that they have no competing interests. **Data and materials availability:** All data needed to evaluate the conclusions in the paper are present in the paper and/or the Supplementary Materials.

Submitted 9 August 2022
Accepted 28 November 2022
Published 4 January 2023
10.1126/sciadv.ade3240

ScienceAdvances

Concurrent stiffening and softening in hydrogels under dehydration

Shuai XuZidi ZhouZishun LiuPradeep Sharma

Sci. Adv., 9 (1), eade3240. • DOI: 10.1126/sciadv.ade3240

Science Advances (ISSN) is published by the American Association for the Advancement of Science. 1200 New York Avenue NW, Washington, DC 20005. The title *Science Advances* is a registered trademark of AAAS.